Development of large-area quadrant silicon detector for charged particles[*]

BAO Peng-Fei(包鹏飞)[1]   LIN Cheng-Jian(林承键)[1;1)]   YANG Feng(杨峰)[1]   GUO Zhao-Qiao(郭昭乔)[2]

GUO Tian-Shu(郭天舒)[2]   YANG Lei(杨磊)[1]   SUN Li-Jie(孙立杰)[1]   JIA Hui-Ming(贾会明)[1]

XU Xin-Xing(徐新星)[1]   MA Nan-Ru(马南茹)[1]   ZHANG Huan-Qiao(张焕乔)[1]   LIU Zu-Hua(刘祖华)[1]

[1] China Institute of Atomic Energy, Beijing 102413, China
[2] Beijing Kelixing Photoelectric Technology Co., Ltd, Beijing 102413, China

Abstract: The quadrant silicon detector, a kind of passivated implanted planar silicon detector with quadrant structure on the junction side, gained its wide application in charged particle detection. In this paper, the manufacturing procedure, performance test and results of the quadrant silicon detector developed recently at the China Institute of Atomic Energy are presented. The detector is about 300 μm thick with a 48 mm×48 mm active area. The leakage current under the full depletion bias voltage of −16 V is about 2.5 nA, and the rise time is better than 160 ns. The energy resolution for a 5.157 MeV α-particle is around the level of 1%. Charge sharing effects between the neighboring quads, leading to complicated correlations between two quads, were observed when α particles illuminated on the junction side. It is explained as a result of distortion of the electric field of the inter-quad region. Such an event is only about 0.6% of all events and can be neglected in an actual application.

Key words: quadrant silicon detector, passivated implanted planar silicon, energy resolution, charge sharing effect

PACS: 07.77.-n, 29.40.Wk   **DOI:** 10.1088/1674-1137/38/12/126001

1   Introduction

Silicon detectors have been widely used in nuclear physics and high energy physics during the past decades thanks to the improvement of modern semiconductor technology [1–4]. With their good energy resolution, fast time response and reliable stability, silicon detectors have been applied to energy spectrum measurement, time signal pickup, and particle identification as well as tracking systems, such as the use in the complete-kinematics measurement of the two-proton emission from extremely proton-rich nuclei [5–7], Silicon Ball for research on the weakly bound nuclei close to the particle drip line [8], and MUST/MUST2 [9, 10] for radioactive beam experiments. Among them, Passivated Implanted Planar Silicon (PIPS) detectors fabricated in the "Planar" process [11, 12] have enjoyed widespread adoption.

PIPS detectors, in most applications, have some advantages over traditional Silicon Surface Barrier (SSB) detectors [1, 2]. All the junction edges of the PIPS detectors are buried in the process of oxide passivation, which can achieve better stability and lower reverse leakage current, while the SSB detectors have crude junction edges. In addition, junctions formed by well controlled ion-implantation provide thin entrance windows and can also reduce the leakage current. A low leakage current guarantees low electronic noise. Moreover, a thin entrance window means a thin dead layer, which brings not only an improvement of energy resolution but also a reduction of energy straggling. Therefore, it enables the possibility of closer detector-source distance to achieve compact geometry and high efficiency [13].

Despite the excellence of their response, however, PIPS detectors have shortcomings as well, especially for ones with a large area. A large capacitor resulting from a large area will in turn lead to a slow rise time and a small voltage output with an equal quantity of charge being ionized. Besides, the detector capacitor is also one of the non-negligible noise causing factors. In the applications that demand time signal pick-up and high signal-to-noise ratio, one can use a quadrant PIPS to replace the large-area one in view of that the area is reduced to a quarter. Quadrant silicon detectors (QSDs) also have other advantages, for instance, a certain position resolution and the reduction of the count rate of readout electronics. There are already commercially available

quadrant silicon detectors [14] and they have been used in ISOLDE Silicon Ball [8].

The QSD has been successfully developed at the China Institute of Atomic Energy (CIAE). The manufacturing procedure, test procedure, and electronics as well as detection performance are presented in detail. Afterwards, the complicated correlations between two neighbouring quads, as a result of charge sharing effects, are discussed.

2　Manufacturing procedure

From the manufacturing point of view, the planar process was developed for producing Integrated Circuits (IC), and it has also been applied to the fabrication semiconductor detectors nowadays [1, 12]. The process is complicated, that combines many crucial techniques such as oxide passivation, photolithography and ion implantation. The whole production flow of our PIPS-QSD goes as follows:

a) Polish and clean. The fabrication of detectors start from a 4 inches, 300 μm thick, high-resistivity (greater than 10 kΩ·cm), high-purity, n-type silicon wafer. The wafer should be polished and cleaned at the beginning.

b) Oxide passivation. The polished Si wafers are passivated by thermal oxidation at temperature up to 1030 ℃. O_2 gas stream flow past the Si wafers and then about 600 nm thick oxide layer (SiO_2) come into being on the wafer surface.

c) Photolithography. Four entrance windows, corresponding to the four quadrants of the finished detector, should be opened. Each one has an area of 24 mm× 24 mm. The oxide layers on those areas are removed with the photolithographic equipment and proper etching techniques.

d) Ion implantation. The junction side is formed by boron ions implantation within the window, while the ohmic side is implanted with phosphorus ions. Therefore, a thin layer of pure silicon on the surface is doped into p-type on the junction side and n-type on the ohmic side, respectively. The proper energy and dose of boron ions are typically 25 keV and 5×10^{14} ions/cm², and 120 keV and 5×10^{15} ions/cm² for phosphorus ions.

e) Annealing. Thermal annealing is one of the most effective methods to remove the radiation damage in the implanted layers in the premise of guaranteeing a low leakage current of detectors. The implanted Si wafers should be annealed in dry N_2 gas at 600 ℃.

f) Al metallization. Both the front and rear surfaces should be evaporated by aluminum for ohmic electrical contacts. The aluminum layer should be very thin, for the energy straggling of incoming particles in the aluminum layer contributes to the noise.

g) Al patterning at the front. The aluminum on the

oxide layers should be removed using a photolithographic technique.

h) Alloy. The aluminum electrode should be alloyed at 380 ℃.

i) Encapsulation. The last step is separating each individual detector and then encapsulating. The detector chip is mounted on the print circuit board (PCB) and the golden wires connect the aluminum electrodes with readout contacts on PCBs using ultrasonic soldering.

The profile view of the QSD is depicted in Fig. 1. The active area of the detector is 48 mm×48 mm, which is divided into four quads (24 mm×24 mm) by a cross SiO_2 bar with 0.1 mm in width.

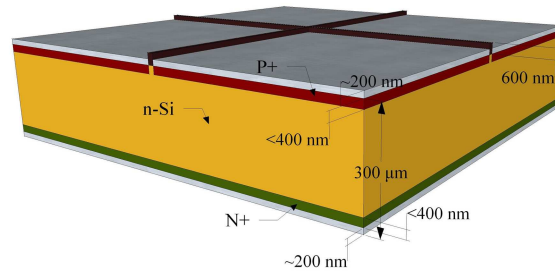Fig. 1.　The profile view of the QSD.

3　Electronics performance

3.1　Electronic setup

The test was performed with ^{241}Am and ^{239}Pu α sources. As shown in Fig. 2, the detector and the preamplifiers were put in a vacuum chamber. α-particles from the radioactive source irradiated the QSD, then the produced charges were collected by the charge sensitive preamplifiers. With the aim of multi-channel integration, low noise and a high signal-to-noise ratio, the preamplifiers were well designed on a PCB to directly connect with detectors. The performance of the preamplifier is excellent, with the bandwidth around 245 MHz and noise better than 5 nV/$\sqrt{\text{Hz}}$. Negative bias voltage was applied to the junction side through a 100 MΩ resistor built in the AC-coupled preamplifier while the ohmic side was directly earthed. The injected charges were integrated on the feedback capacitor into a current pulse, which was then shaped by a spectroscopy amplifier, CAEN N1568A. Timing signals were produced by the built-in constant fraction discriminator (CFD) of the amplifier, as a trigger to generate the gate signal for V785 ADC. Based on the VME data acquisition system, V785 ADC converted the height of pulse into a digital signal to save on a PC for further data analysing. The sequence of the number of four quads is also shown in Fig. 2. Hereinafter, we call Quad.1 Q1 for convenience, and the same for the others.
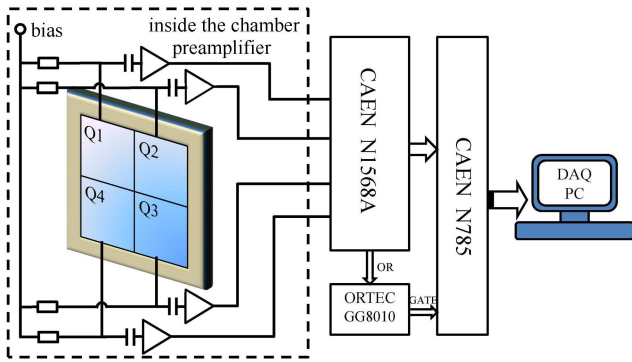
Fig. 2.   A block diagram of the electronic setup.

3.2   Leakage current

The bias voltage applied to the detector is supplied by a Keithley 2602A Source Meter; the total leakage currents of four quads can be measured simultaneously. Fig. 3 presents the curve of leakage currents of the QSD as a function of the bias voltage. The test was performed at room temperature 25 ℃. When the detector is fully depleted at the bias voltage −16 V, the leakage current of each quad is as low as 2.53 nA. Even under the bias of −20 V, the leakage of each quad is merely 5.01 nA. During the whole test procedure, the leakage currents are roughly constant, showing a good stability.
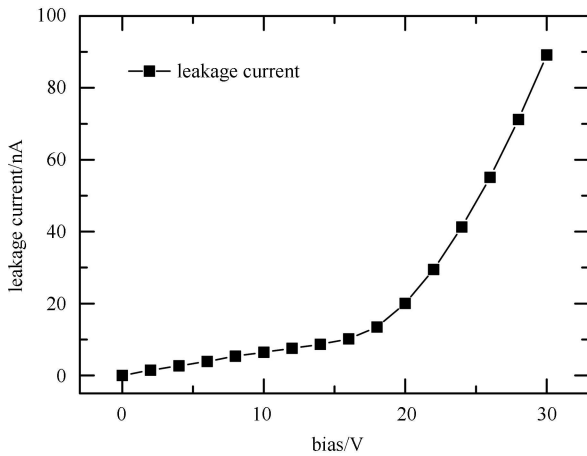

Fig. 3.   I-V curve of the QSD. The leakage currents are plotted as a function of bias voltage. The leakage currents here are the sum of currents from four quads.

Leakage current is a significant factor that should be considered for operating almost all the semiconductor junction detectors. For one thing, great magnitude of leakage currents could bury weak signals to be measured. For another, fluctuations of the leakage currents contribute to the electronic noise, which broaden the overall peak and consequently reduce the energy resolution. It is known that leakage currents originate from the surface and bulk volume of the detector. The bulk leakage results from the diffusion of the minority carriers and the thermal generation of electron-hole pairs, both of which show little connection with the manufacturing process. Different from this, surface leakage currents, related to the large voltage gradient at the junction edges, are dependent on the encapsulation of the detector and the contamination on the detector surface. From this point of view, the low level of leakage currents of these QSDs represents the fabrication process technic level of the detector to some extent.

3.3   Energy and timing responses

The output energy signals of preamplifiers generated by α-particles illuminating onto the detector are injected into an oscilloscope, thus the pulse amplitude and rise time measurements are accessible. The upper panel in Fig. 4 shows the pulse amplitude and rise time as a function of reverse bias voltage when α particles irradiate on the junction side of the detector. The bias increases with a step of 2 V from 0 V to −30 V. As shown in Fig. 4, the pulse goes high and rises fast while the bias goes up from 0 V to −10 V. Once the bias is increased over −12 V, the pulse height is roughly constant and remains 89 mV while the rise time decreases slowly and levels off at higher voltage.
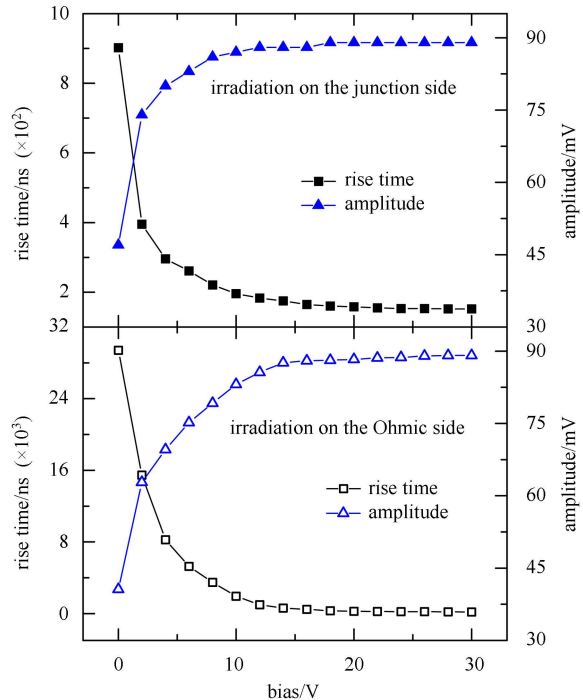

Fig. 4.   The upper panel shows the pulse amplitude and rise time as a function of reverse bias voltage when α particles irradiate on the junction side of the detector, while the lower panel for α particles irradiating on the Ohmic side.

As the range of 5 MeV α particles in silicon is about 30 μm, just a tenth of the whole thickness of Si bulk, it may not be persuasive to determine the full depletion of the p-n junction simply according to the signals from incidence on the junction side. The lower panel in Fig. 4 presents the same curves but α particles irradiating on the ohmic side. In this case, under the bias less than -10 V, the rise time of that signal is rather slow and the pulse height is slightly small in contrast with the situation of illumination on the junction side. Obviously, it is a result from the weak electric field near the ohmic side. The pulse height gets to be saturated and the rise time grows slowly until the bias increases to -16 V, under which bias voltage, we can conclude, the p-n junction is fully depleted. Considering that the detector should be over-depleted, we applied the bias voltage of -20 V across the detector during the test. Under this bias, the rise time of signal of ^{241}Am α particles is 158 ns.

4   Detection performance

4.1   Energy resolution

Figure 5 presents a typical α particle energy spectrum of ^{239}Pu source. The two peaks are corresponding to 5.157 MeV and 5.499 MeV [15], respectively. The peak of 5.499 MeV is caused by the mixed ^{238}Pu, and the peak of 5.157 MeV contains the contributions from 5.144 MeV and 5.106 MeV α particles with small branch ratios which cannot be distinguished. After the single-peak Gaussian fit of the 5.157 MeV peak, one can calculate that the $\sigma = 10.484$ Ch and the peak is located at 2545.8 Ch, resulting in the energy resolution of 0.97%. That is to say, the energy resolving capability is about 50 keV. The energy resolution was relatively consistent across the four quads with a difference less than 5% off
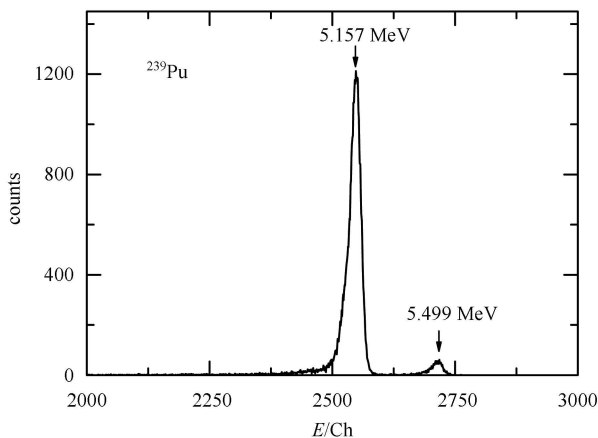
the average. Considering that the α source is too close (about 8 cm) to the detector that the incident angle tends to vary largely so as to increase the energy straggling, the energy resolution may improve under the condition of the vertical incidence after collimation. The performance of energy resolution is acceptable.

It is the good energy resolution that is the most dramatic factor of the silicon detector; it ensures the wide applications of these detectors on energy spectrum measurements and particle discrimination. Energy resolution depends on many physical factors, not only the detector itself, but also the front-end electronics system and even the energy and mass of the charged particle to be detected. If the impacts of system energy resolution are excluded, the intrinsic energy resolution of the detector should be better than 50 keV.
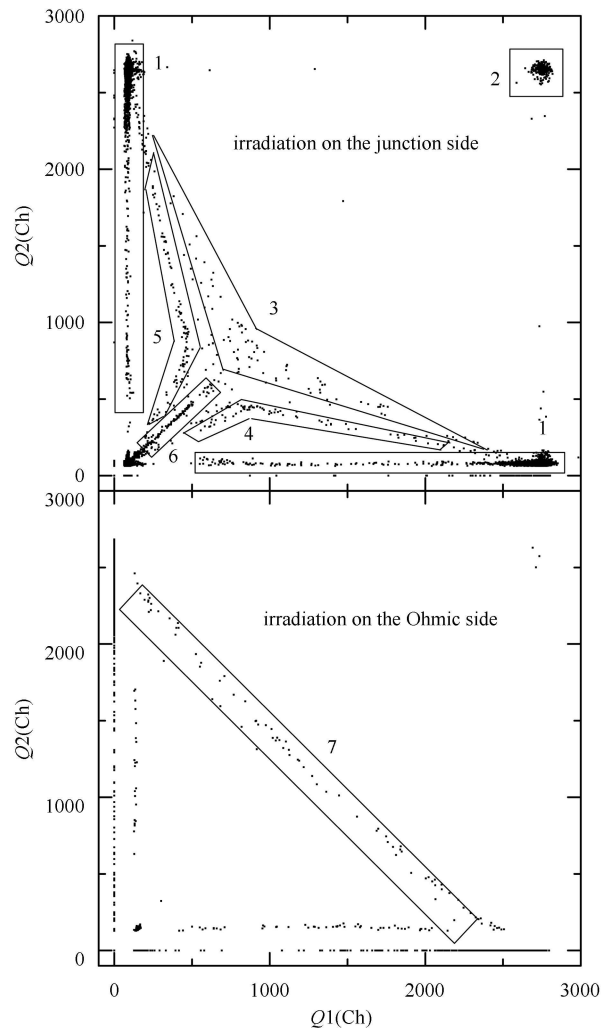

Fig. 6.   Typical correlation spectrum of ^{241}Am α particles between two neighbouring quads on the same QSD, the upper panel for α particles irradiating on the junction side and the lower panel for the ohmic side. See the context for more details about the origination of these correlations.

Fig. 5.   Typical ^{239}Pu α particles energy spectrum of the QSD. The two peaks are corresponding to 5.157 MeV and 5.499 MeV, respectively, with an energy resolution of 0.97%.

4.2   Charge collection analysis

Figure 6 shows a typical correlation spectrum of ^{241}Am α particles between two neighbouring quads on the same QSD, the upper panel for α particles irradiating on the junction side and the lower panel for the ohmic side. A charge sharing effect [16–18] can be observed from both of them. For convenience of expression, the spectrum are divided into seven zones.

In the upper panel, the vast majority of events (in Zone 1, almost 98.9% of all effective events) shows the two quads records α particles independently in addition to few accidental coincidence events (in Zone 2, about 0.4%). There are also a tiny number of events (in Zone 3, 4, 5, and 6, about 0.6%) that show complicated correlations between the two quads. The active area of the detector is 48 mm×48 mm, and the width of the isolation bar is 0.1 mm, then one can get that the ratio of the dead zone to the active zone is $(0.1+0.1)\div48=0.42\%$. From its consistence with the ratio of the number of correlation events to that of total events, one can surmise that the correlation may be caused by events that α particles incident on the inter-quad area.

It encourages us to do further test to search out the origination of these correlation events. As shown in Fig. 7, a different part of the detector was masked by a thick paper board with a window at different position to let α particles merely irradiate on a specific area, events from which can be distinguished therefore.

In Fig. 7(a), only part of one quad was irradiated.

This test shows that there is no correlation observed between any two quads. The spectrums of three non-irradiated quads were blank except noises in extremely low channels. It is concluded that the front-to-end electronic crosstalk can be neglected and the effects of capacity coupling were not observed.
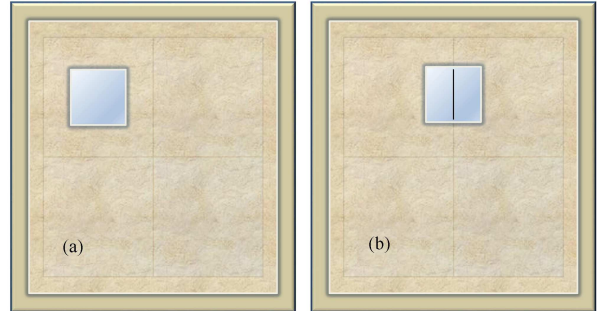

Fig. 7.   Two test modes with a windowed thick paper board masking a different part of the detector. The light blue area can be irradiated by α particles. During these tests, the α source faced the window to avoid oblique incidence.

As for Fig. 7(b), part of the inter-quad region between two quads was irradiated, and events originated from this region can be studied. Four panels in Fig. 8 present the scatter plots of different pairs of the four quads. In Fig. 8(a), a symmetrical broken-line of the spectrum of $Q1$ vs $Q2$ is presented. Obviously, charges ionized
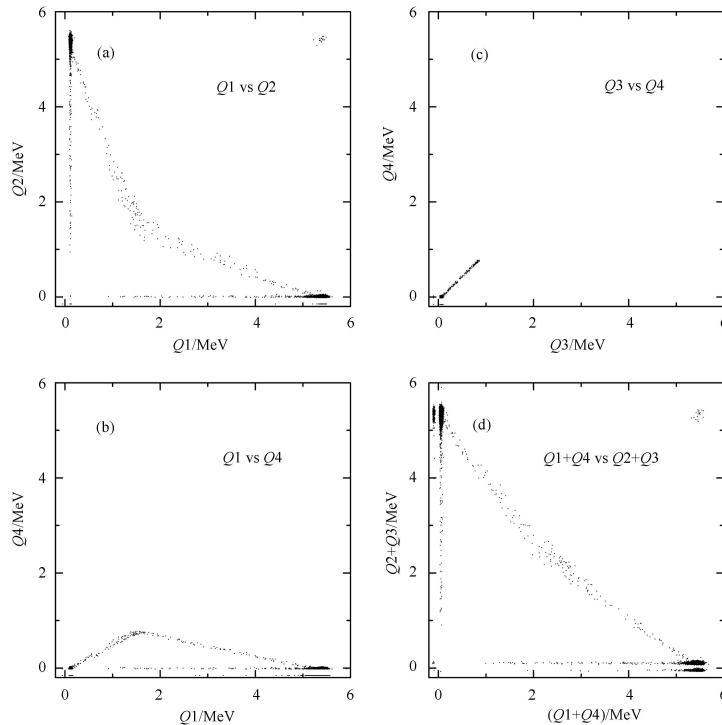

Fig. 8.   Correlation spectrum of test in Fig. 7(b).

by α particles that irradiated on the inter-quad region are not collected completely by $Q1$ and $Q2$, otherwise the spectrum of the two quads should be a straight line $E_{Q1}+E_{Q2}=E_{\mathrm{tot}}$. Furthermore, the closer to each other the values of $Q1$ and $Q2$ become, the greater quantity of charges they lose. The lost charges are collected by $Q3$ and $Q4$, as will be further discussed below. That is certainly corresponding to the events in Zone 3 of Fig. 6.

From the plot of $Q1$ vs $Q4$ in Fig. 8(b), one can find out that $Q4$ gets to its maximum at the turning point of the broken line of $Q1$ vs $Q2$, meaning that $Q4$ collects a maximum amount of charge when $Q1$ and $Q2$ lose the most. It can be concluded that charges are shared by four quads even α particles just incident on the inter-quad region between two quads. It is similar to the events in Zone 4 and Zone 5 of Fig. 6. Zone 4 is composed of events that α particles irradiated on the inter-quad area between $Q1$ and $Q4$, and the charges are partly collected by $Q2$. Likewise, events in Zone 5 stand for α particles irradiating between $Q2$ and $Q3$, and part of the charges are collected by $Q1$.

The plot of $Q3$ vs $Q4$ is given out in Fig. 8(c). What puzzled us a lot is that $Q3$ always collected the same quantity of charges as $Q4$. It may be understood that the charges ionized at the inter-quad region between $Q1$ and $Q2$ may not only be collected by $Q1$ and $Q2$, but also drift along the long inter-quad insolation strip and finally be bisected by $Q3$ and $Q4$. Homologous events in Fig. 6 are located in Zone 6, that charges are ionized between $Q3$ and $Q4$, and part of them drifting along the SiO_2 isolation strip are equally shared by $Q1$ and $Q2$ finally.

In order to further verify this, we give out the spectrum of $Q1+Q4$ vs $Q2+Q3$ in Fig. 8(d), the correlation between these two parameters are closer to the straight line. According to this fact, it can be concluded that most of the charges are shared by the quads on both sides of the isolation strip, and only a small part of charge was lost during the collection.

Unlike the case in the upper panel of Fig. 6, events

of α particles irradiating on the ohmic side do not have complex correlations. The straight line in Zone 7 represents events that charges are completely collected by two neighbouring quads, but not shared by four quads.

Conclusions can be made based on different phenomenons of the irradiation on two sides of the detector, that the electric field distortion occurs in the inter-quad regions, and only near the surface of the junction side. α particles irradiate on the inter-quad region between two quads on the junction side and the ionized charges are affected by the distorted electric field and partly collected by the other two quads. While irradiation take place on the ohmic side, α particles cannot feel the electric field distortion before being stopped, and the ionized charges were completely collected.

Generally speaking, the amount of inter-quad events are small enough to be neglected in practical use of the experiments.

5   Summary

The QSDs for charged particle detection were developed at the China Institute of Atomic Energy. The thickness of the QSD is about 300 μm and the active area is 48 mm×48 mm with a 0.1 mm wide isolation bar between each two quads. Tests with ^{241}Am and ^{239}Pu radioactive sources were carried out to assess the performance of the detector. The leakage current under the over-depletion bias voltage of -20 V is as small as 5.01 nA, and the rise time is better than 160 ns. The energy resolution for 5.157 MeV α-particle is about 1%. The analysis results show the existence of complicated correlations between neighboring quads, which are caused by the electric field distortion near the isolation bar. The inter-quad events would not impact too much as the amount of these events is tiny. These performances are acceptable. In view of the fabrication reaching such a level that these detectors can be used in nuclear physics experiments, one should also consider the long term behaviour of these detectors, such as radiation damage and electrical stability.

References

1 Knoll G F. Radiation Detection and Measurement. fourth edition. Hobeken, NJ: John Wiley & Sons Inc. 2010. 365–414
2 Lutz G. Semiconductor Radiation Detectors. New York: Springer, 1999. 95–108
3 Davinson T, Bradfield W, Cherubini S et al. Nucl. Instrum. Methods A, 2000, **454**: 350
4 Walton J T. Nucl. Instrum. Methods, 1984, **226**: 1
5 LIN C J, XU X X, JIA H M et al. Phys. Rev. C, 2009, **80**: 014310
6 XU X X, LIN C J, JIA H M et al. Phys. Rev. C, 2010, **81**: 054317
7 XU X X, LIN C J, JIA H M et al. Phys. Lett. B, 2013, **727**: 126
8 Fraile L M, Äystö J. Nucl. Instrum. Methods A, 2003, **513**: 287
9 Blumenfeld Y, Auger F, Sauvestre J E et al. Nucl. Instrum. Methods A, 1999, **421**: 471
10 Pollacco E, Beaumel D, Roussel-Chomaz P et al. Eur. Phys. J. A, 2005, **25**: 287
11 Kemmer J. Nucl. Instrum. Methods, 1980, **169**: 499
12 Kemmer J. Nucl. Instrum. Methods A, 1984, **226**: 89
13 Bergmann U C, Fynbo H O U, Tengblad O. Nucl. Instrum. Methods A, 2003, **515**: 657
14 http://www.micronsemiconductor.co.uk/
15 Rytz A. At. Data and Nucl. Data Tables, 1991, **47**: 205
16 Poehlsen T, Fretwurst E, Klanner R et al. Nucl. Instrum. Methods A, 2013, **700**: 22
17 Yorkston J, Shotter A C, Syme D B et al. Nucl. Instrum. Methods A, 1987, **262**: 353
18 Grassi L, Torresi D, Acosta L et al. AIP Conference Proceedings, 2012, **1491**: 135